EFFECTS OF ELECTRODE DISTANCE AND TARGET ANGLES ON ELEMENTAL CONCENTRATIONS AND FILM PROPERTIES OF AL-DOPED ZNO FILMS PREPARED BY MAGNETRON CO-SPUTTERING

Angelika Gorgulla, Kay Hagedorn, Giso Hahn, Barbara Terheiden
University of Konstanz, Department of Physics, 78457 Konstanz, Germany
Phone: +49 7531 88 2080, Fax: +49 7531 88 3895, Email: angelika.gorgulla@uni-konstanz.de

ABSTRACT: We investigate the effects of Al and Zn target angles and electrode distance on the elemental concentrations, as well as on the electrical, optical and structural properties of Al doped zinc oxide (ZnO:Al) films prepared by RF magnetron co-sputtering. To obtain the Al and Zn concentrations, inductively coupled plasma optical emission spectrometry (ICP-OES) is used. With increasing Zn target angle from 8 to 24° (0° corresponds to target plane parallel to substrate surface) electrical resistivity is reduced by over three orders of magnitude, and an increase of Al target angle from 0 to 24° allows a reduction by a factor of 7. As a result, resistivities below $2 \cdot 10^{-3}$ Ωcm are obtained. This decrease of resistivities is a consequence of improved crystallinity and lower defect density, leading to increased charge carrier density and mobility. In addition, the increase of Al target angle allows increasing the average transmission within the VIS range (400-800 nm) from 49 to 79%. Optimizing Al and Zn target angles therefore allows significant improvement of the electrical and optical film properties.
Keywords: TCO, AZO, ZnO:Al, heterojunction solar cells, magnetron sputtering, oblique angle deposition

1 INTRODUCTION

Al-doped zinc oxide (ZnO:Al) thin films are of interest in numerous PV applications, e. g. a-Si:H/c-Si heterojunction and thin film solar cells, due to their features such as a high transmittance within the UV, VIS and NIR as well as low electrical resistivity in the order of 10^{-3} to 10^{-4} Ωcm. ZnO:Al as transparent conducting oxide (TCO) is a promising alternative for the still widely used, but much more costly indium tin oxide (ITO).

Oblique angle sputter deposition has been found to allow the fabrication of ITO and ZnO thin films with improved optical properties and film uniformity [1,2]. While numerous studies exist investigating the effects of deposition parameters such as substrate temperature, working pressure, rf/dc power and O_2 flow on the properties of Al-doped ZnO films, few have been found addressing the effects of target angle, and none of the investigated films were prepared by co-sputtering. Purpose of this study is therefore to investigate the effects of Al and Zn target angles on the elemental concentrations as well as the optical, electrical and structural film properties. As a variation of target angle also inflicts a change of the effective electrode distance (spacing between substrate holder and sputtering targets), we include this deposition parameter in our investigations. To obtain the Al and Zn concentrations ICP-OES [3] is used, which is a novel approach of measuring elemental concentrations in ZnO films [4].

2 EXPERIMENTAL

ZnO:Al films were deposited at room temperature on float-zone Si (for ellipsometry measurements) and borofloat glass (for all remaining measurements) at room temperature in a radio-frequency rf-13.56 MHz magnetron sputtering system (ATC-2200, AJA International) by reactive co-sputtering using metallic Zn (300 W) and Al targets (255 W) of 99.99% purity. Argon (20 sccm) and O_2 (7.5 sccm) were used as sputtering gas, with a working pressure of 0.5 mTorr. During deposition, the substrates were rotated with constant speed for film uniformity.

To investigate the influence of deposition parameters on film properties systematically, three sets of films were prepared by changing a specific deposition parameter at a time, with the others remaining constant. The Al target angle was varied from 0 to 40° (0° corresponds to target plane parallel to substrate), the Zn target angle from 8 to 40°, and the electrode distance from 12.5 to 19.5 cm (distance referring to 0° position of target angles). Unless noted otherwise, the electrode distance was fixed at 14.2 cm, and the Zn and Al target angles positioned at 24°. Fig. 1 shows a schematic of the used sputtering set-up.

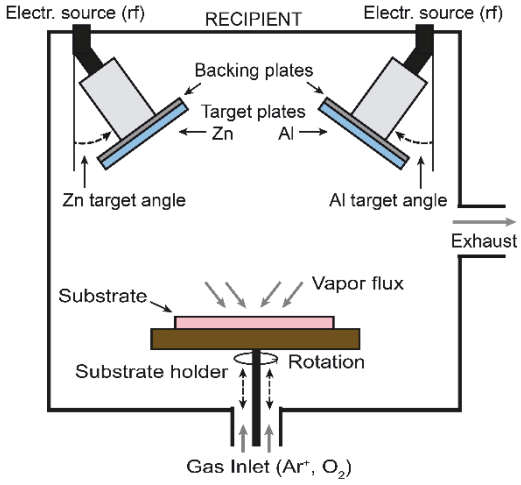

Figure 1: Schematic of the RF magnetron co-sputtering chamber set-up with variable Zn an Al target angles and adjustable substrate position or electrode distance, respectively.

Pior to the sputtering process, all substrates were ultrasonically cleaned in acetone, isopropanol and deionized water sequentially. Afterwards, the substrates were dried with nitrogen gas. Before deposition, the sputtering chamber was evacuated to a base pressure of less than 10^{-6} Torr. After a pre-sputtering period of 2 min under deposition conditions, the sputtering deposition was performed.

Electrical resistivity, free carrier density, and carrier mobility of the films were derived from Hall measurements at room temperature using the van der Pauw method. Optical properties were characterized by spectral transmission and reflection measurements within a wavelength range of 300-2500 nm taken by a spectral photometer. The optical constants (n, k) and optical bandgaps E_{gap} were deduced from spectral ellipsometry measurements between 250-1100 nm. The optical band gap was calculated from the fitted data by using Tauc's formula [5]. For ICP-OES (720 series, Agilent) element analysis, the ZnO:Al films were dissolved in 0.5%$_{abs}$ hydrofluoric acid. The ratio of Zn and O was determined by energy dispersive X-ray spectrometry (EDX) measurements. The crystalline structure of the films was analyzed by X-ray diffraction (XRD) (D8 XRPD, Bruker) using Cu K_α radiation (0.1542 nm). The mean grain size of the films is derived from Scherrer's equation [6] using the (002) diffraction peak.

3 RESULTS AND DISCUSSION

3.1 Electrode distance

The deposition rate, which is proportional to the amount of target materials supplied, decreases slightly from 5.6 to 4.7 Å/s as the electrode distance is increased from 12.5 to 19.5 cm (not shown).

ICP-OES measurements show (Fig. 2), that the Al concentration c_{Al} decreases from 4.7 to 3.8 cm^{-3} within the film, while the Zn concentration c_{Zn} stays almost constant. The reduced Al concentration causes a decrease of charge carrier density N_e from $1.3 \cdot 10^{20}$ to $5.0 \cdot 10^{19}$ cm^{-3} (Fig. 3). The fraction of Al atoms effectively acting as dopants N_e/c_{Al} (Fig. 2), which can be considered a measure for the defect density within the films, seems to be correlated to charge carrier mobility μ_e (Fig. 3). Both decrease below a distance of 14 cm, which is likely due to effects of plasma damage. At higher distance they both decrease, which may be ascribed to the increased deposition rate, as with higher deposition rate the ad-atoms have less time to move on the film surface and to find an energetically stable position with optimum bonding configuration to the adjacent film atoms. As a result, the resulting film would have more defects with poorer crystallinity. This assumption is also supported by XRD measurements.

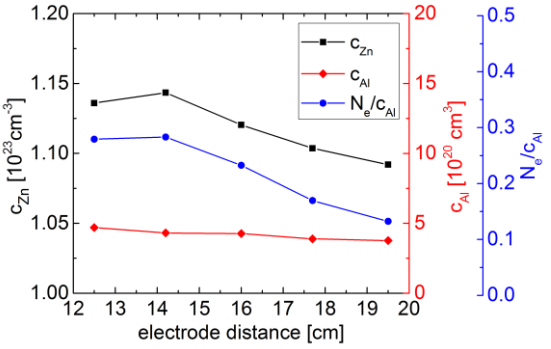

Figure 2: Zn concentration c_{Zn}, Al concentration c_{Al} and fraction of Al atoms effectively acting as donors N_e/c_{Al} versus electrode distance.

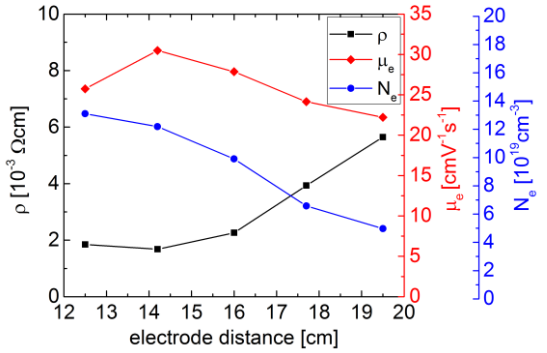

Figure 3: Electrical resistivity ρ, mobility μ_e and charge carrier density N_e versus electrode distance.

All films are polycrystalline with a c-axis ZnO (002) preferential orientation perpendicular to the substrate surface. The intensity of the (002) diffraction peak and the mean grain size derived from Scherrer's equation [6] are depicted in Fig. 4. The film deposited at an electrode distance of 14.2 nm, which achieved the highest mobility and lowest defect density, also features largest grain size and highest peak intensity. The superior electrical properties can therefore be attributed to the highest degree of crystallinity. Electrical resistivity of less than $1.9 \cdot 10^{-3}$ Ωcm is obtained at small electrode distances between 12.5 to 14.2 cm (Fig. 3).

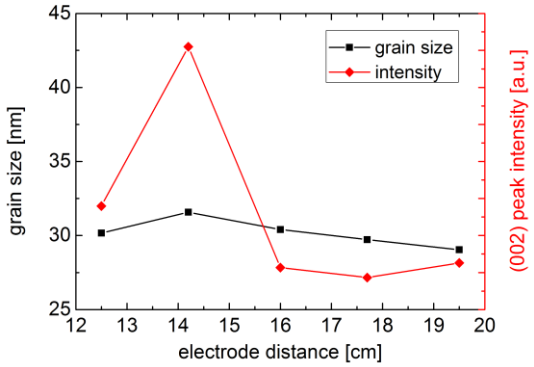

Figure 4: (002) peak intensity of XRD spectra and grain size derived from Scherrer's equation in dependence of electrode distance.

Optical transmission spectra and bandgap energies for various electrode distances are plotted in Fig. 5.

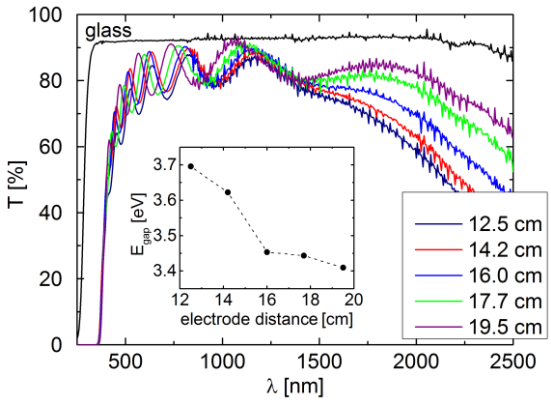

Figure 5: Transmission spectra and optical band gaps for various electrode distances.

The bandgap energy decreases monotonously from 3.70 to 3.41 eV due to the Burstein-Moss-effect. The increase of transmission within the long-wavelength range (> 1000 nm) with higher electrode distance is a result of reduced free carrier absorption.

3.2 Zn target angle

The deposition rate increases from 1.1 to 6.9 Å/s as the Zn target angle is increased from 8 to 40° (Fig. 6).

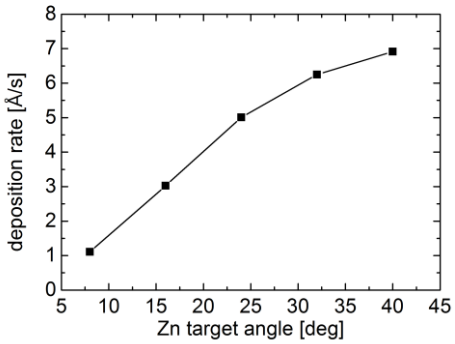

Figure 6: Deposition rate versus Zn target angle.

The explanation for the strong increase is that at smaller angles an increasing fraction of sputtered atoms misses the substrate. At 0° it was not possible to deposit films within reasonable deposition times and therefore this angle position was omitted. As the deposition time was kept constant for all depositions, the thickness of the films varies from 130 to 830 nm, which has to be taken into consideration for discussion of the film characteristics.

While Zn concentration varies only slightly as Zn target angle is increased from 8 to 40°, the Al concentration is strongly reduced from $1.7 \cdot 10^{21}$ to $3.1 \cdot 10^{20}$ cm^{-3} (Fig. 7). This can be explained by the increased deposition rate of Zn, while the deposition rate of Al remains constant. The increase of Al atoms at smaller Zn target angles, however, does not lead to an increase of the charge carrier density, as shown in Fig. 7. N_e/c_{Al} decreases from above 0.43 at 32° to below 0.01 at 8° (Fig. 7). The mobility behaves in a similar manner (Fig. 8), i. e. it is constant between 24 and 40° at around 24 cm^{2}V^{-1}s^{-1} and decreases down to 0.36 cm^{2}V^{-1}s^{-1} at 8°, which is presumably a consequence of increased defect scattering.

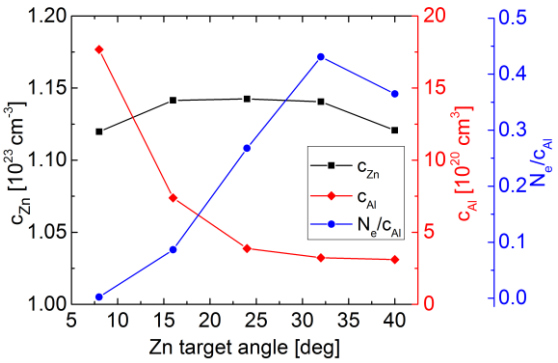

Figure 7: Zn concentration c_{Zn}, Al concentration c_{Al} and fraction of Al atoms effectively acting as donors N_e/c_{Al} versus Zn target angle.

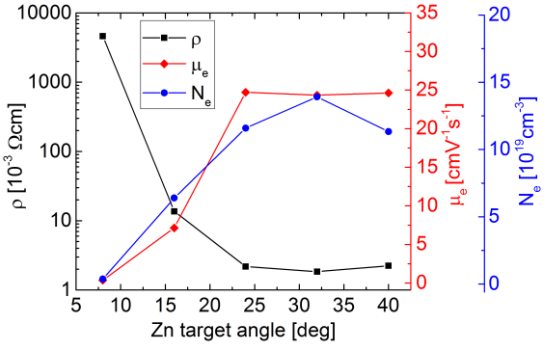

Figure 8: Electrical resistivity ρ, mobility μ_e and charge carrier density N_e versus Zn target angle.

Decrease of mobility and carrier density lead to an increase of resistivity over three orders of magnitude from over 1 Ωcm to around $2 \cdot 10^{-3}$ Ωcm. It could have been assumed, that the strong decrease of sputtering rate at smaller Zn target angle would improve the electrical properties; with slower deposition rate the ad-atoms have more time to move on the film surface to find an energetically stable position with optimum bonding configuration to the adjacent film atoms, so that the resulting film would have a denser structure with higher crystallinity and lower resistivity. However, there are several explanations, why this is not observed. Firstly, the smaller film thicknesses at lower Zn target angles might be responsible for the deteriorated electronic film properties. It has been shown for ZnO thin films, that decreasing thickness results in increased structural disorder, which results in smaller grain sizes and therefore higher electric resisitivity [7]. A further explanation is the strong increase of Al concentration from $3.1 \cdot 10^{20}$ up to $1.7 \cdot 10^{21}$ cm^{-3}, which may enhance doping related defect formation and result in the observed decrease of defect density respectively N_e/c_{Al}. A further explanation could be that the incidence angle of sputtered target molecules is in fact a determining parameter for the change of the electrical properties. It has been shown previously, that different incidence angles can affect the ad-atom mobility and film growth behavior due to an enhanced shadowing effect [8]: In case of a nearly vertical incident angle, momentum transferred by plasma ions is very small so that the ad-atoms gain weak surface mobility. The momentum transfer is larger in case of larger incident angles, with the result that the ad-atoms get a higher chance for arriving at the film growth front and incorporating into the larger grains. However, this thesis is not supported by our XRD results.

The XRD measurements show, that all films are polycrystalline with a c-axis ZnO (002) preferential orientation perpendicular to the substrate surface independent of Zn target angle. The grain size increases from 28 to 42 nm with increasing Zn target position from 8 to 16°, but remains at relatively constant value above 16° (Fig. 9). The intensity, on the other hand, shows a correlation to N_e/c_{Al}, suggesting that at Zn target angle below 24° both defect and grain boundary scattering are responsible for the strong decrease in mobility.

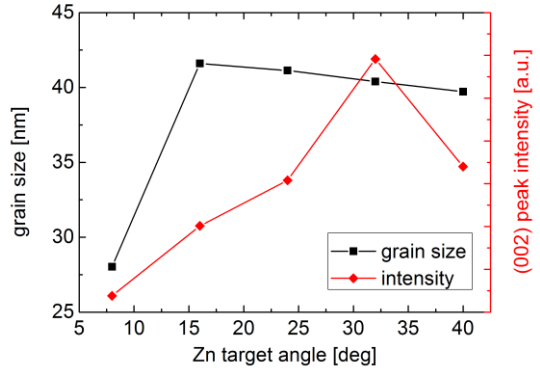

Figure 9: (002) peak intensity of XRD spectra and grain size derived from Scherrer's equation in dependence of Zn target angle.

Optical transmission spectra and optical bandgap energies for various Zn target angles are shown in Fig. 10. Within the VIS range, the differing film thicknesses become apparent in varying interferences. In the long wavelength range above 1500 nm, free carrier absorption results in a decrease of transmission with increasing carrier density. The optical bandgap widens with increased carrier concentration due to the Burstein-Moss-Effect.

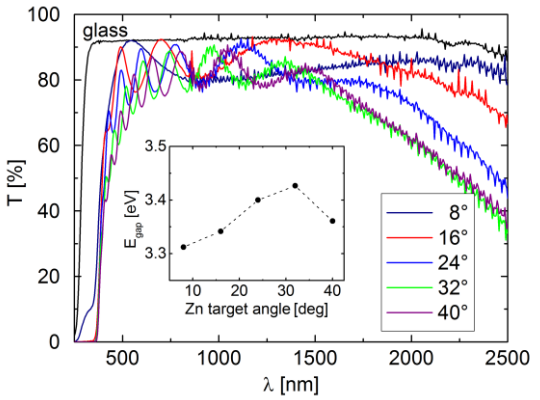

Figure 10: Transmission spectra and optical bandgaps for various Zn target angles.

3.3 Al target angle

The deposition rate remains between 54-55 Å/s unaffected from the Al target angle. As the Al target angle is increased from 0 to 15°, the Al concentration in the ZnO:Al increases from 1.5 to 4.0 cm^{-3}. With further increase of Al target angle, the Al concentration decreases slightly and levels out at 4.0 cm^{-3} (Fig. 11). The Zn concentration increases for Al target angles up to 24° and decreases for higher Al target angles (Fig. 11). This trend is similar to the behaviour of charge carrier mobility (Fig. 12). The decrease of mobility and carrier density might be associated with an increase in effective electrode distance, which also leads to an increase of resistivity. Lowest electrical resistivity ρ is obtained at an Al target angle between 16-24° (Fig. 12).

XRD measurements show, that all films retain the polycrystalline structure with a c-axis ZnO (002) preferential orientation perpendicular to the substrate surface for Al target angles. No significant impact on the grain size or crystallinity of the films can be observed (not shown). The grain size of the films is in the range of 29 to 31 nm for all films.

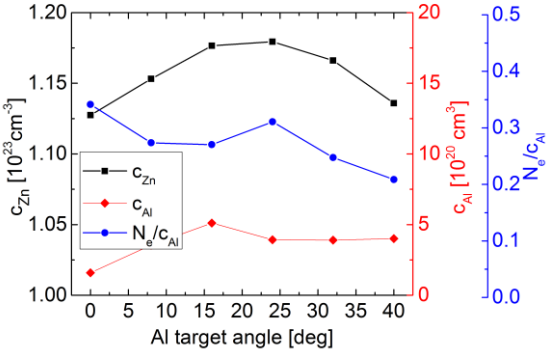

Fig. 11: Zn concentration c_{Zn}, Al concentration c_{Al} and fraction of Al atoms effectively acting as donors N_e/c_{Al} versus Al target angle.

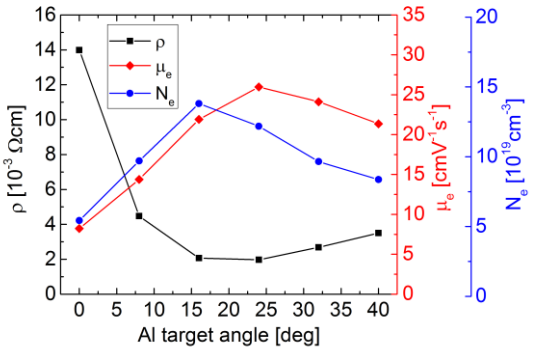

Figure 12: Electrical resistivity ρ, mobility μ_e and charge carrier density N_e versus Al target angle.

Optical transmission spectra and optical bandgap energies for various Al target angles are plotted in Fig. 13. The bandgap energy resembles the trend of the charge carrier density due to the Burstein-Moss-Effect. Within the VIS-range (400-800 nm), the average transmission increases significantly from 49 to 79%. In the long wavelength-range (> 1000 nm), the impact of free carrier absorption can be observed.

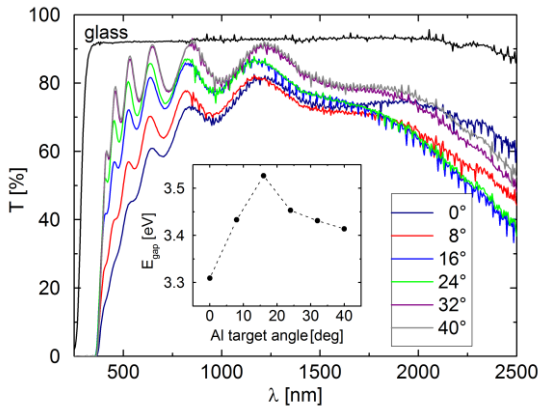

Figure 13: Transmission spectra and optical bandgaps for various Al target angles.

4 CONCLUSION

We have investigated the impact of Al and Zn target angles as well as the electrode distance on the elemental concentrations and film properties of co-sputtered ZnO:Al. The target angles have a significant impact on the

film properties, which cannot be simply explained by the change in electrode distance inflicted during target angle variation. By optimizing Al and Zn target angle it is possible to significantly improve the electrical and optical film properties.

ACKNOLEDGEMENTS

Part of this work was financially supported by the German Federal Ministry for Economic Affairs and Energy (FKZ 0325581) and within the "REFINE" project from the Carl-Zeiss-Stiftung. The content is the responsibility of the authors.

REFERENCES

[1] Y. Zhong et al., J. Mater. Res. 23 (2008) 2500.
[2] Park et al., J. Nanosci. Nanotechno. 14 (2014) 7710.
[3] S. Ghosh et al., Asian J. Pharm. Ana. 3 (2013) 24.
[4] A. Gorgulla et al., Energy Procedia 77 (2015), 687.
[5] J. Tauc et al., J. Non-Cryst. Solids 8 (1979) 569.
[6] P. Scherrer, Göttinger Nachrichten Gesellschaft. 2 (1918) 98.
[7] E. Ş. Tüzemen et al., Appl. Surf. Sci. 255 (2009) 6195.
[8] S. H. Lee et al., Curr. Appl. Phys. 10 (2010) 286.